

Multi Order Coverage data structure to plan multi-messenger observations

Giuseppe Greco¹, Michele Punturo

INFN, Sezione di Perugia, I-06123 Perugia, Italy

Mark Allen, Ada Nebot, Pierre Fernique, Matthieu Baumann, François-Xavier Pineau, Thomas Boch, Sébastien Derriere

Université de Strasbourg, CNRS, Observatoire astronomique de Strasbourg, UMR 7550, F-67000, Strasbourg, France

Marica Branchesi

Gran Sasso Science Institute (GSSI), Aquila, Italy

INFN, Laboratori Nazionali del Gran Sasso, I-67100 Assergi, Italy

Mateusz Bawaj, Helios Vocca

Università degli Studi di Perugia, Perugia, Italy

INFN - Sezione di Perugia, Italy

Abstract

We describe the use of Multi Order Coverage (MOC) maps as a practical way to manage complex regions of the sky for the planning of multi-messenger observations. MOC maps are a data structure that provides a multi-resolution representation of irregularly shaped and fragmentary regions over the sky based on the HEALPix (Hierarchical Equal Area isoLatitude Pixelization) tessellation. We present a new application of MOC, in combination with the **astropplan** observation planning package, to enable the efficient computation of sky regions and the visibility of these regions from a specific location on the Earth at a particular time.

Using the example of the low-latency gravitational-wave alerts, and a simulated observational campaign with three observatories, we show that the use of MOC maps allows a high level of interoperability to support observing schedule plans. Gravitational-wave detections have an associated credible region localization on the sky. We demonstrate that these localizations can be encoded as MOC maps, and how they can be used in visualisation tools, and processed (filtered, combined) and also their utility for access to Virtual Observatory services

¹giuseppe.greco@pg.infn.it

which can be queried 'by MOC' for data within the region of interest. The ease of generating the MOC maps and the fast access to data means that the whole system can be very efficient, so that any updates on the gravitational-wave sky localization can be quickly taken into account and the corresponding adjustments to observing schedule plans can be rapidly implemented. We provide example python code as a practical example of these methods. In addition, a video demonstration of the entire workflow is available.

Keywords: multi-messenger, gravitational waves, multi order coverage map, sky localization, visibility

1. Multi-messenger data science tools and worldwide collaborations

The first discovery of gravitational waves from the coalescence of two neutron stars in a binary system, GW170817, was made by the LIGO and Virgo collaboration (LVC) [1] during the second observational run of LVC [2]. The subsequent identification of its electromagnetic counterpart, GRB170817 / AT2017gfo, has ushered the science community in the era of multi-messenger astronomy [3].

During the LVC third observing run new data science tools have been developed, and worldwide collaborations have been organised to support coordinated follow-up observations and their analysis, see [4] and references therein. The future growth of multi-messenger astronomy that is expected in the next decades [5], [6] will require an appreciable coordination effort and a significant synergy between different ground-based observatories, space-borne satellites and second/third-generation interferometric gravitational wave detectors (Virgo [7], LIGO [8], KAGRA [9], Cosmic Explorer [10], Einstein Telescope (ET) [11]).

The establishment of the interoperable infrastructures that will be needed to support observatory operations, astronomical research, and data storage, are achievable goals if the active multi-messenger community cooperates in the development of technical standards and common protocols. The International Virtual Observatory Alliance (IVOA) [12] is an organisation that develops the technical standards to lay the foundation of the astronomical Virtual Observatory (VO) [13], [14], [15]. A number of VO-based protocols are being developed and updated to respond to the needs of multi-messenger astronomy. For example, two of the protocols in development for the planning of multi-messenger observations [16] are: *(i)* the Observation Locator Table Access Protocol (ObsLocTAP)² to define a data model for observation schedules, and *(ii)* the Object Visibility Simple Access Protocol (ObjVisSAP)³ for retrieving the visibility of astronomical objects (based on their sky coordinates) through a uniform query interface. These protocols are expected to be very useful for the planning of observations in the cases where object coordinates are known, or where the planning can be done point by point.

²<https://github.com/ivoa-std/ObsLocTAP>

³<https://github.com/ivoa-std/ObjVisSAP>

In this article, we consider the cases where astrophysical sources may be localised in relatively large sky regions, and in particular the case of multi-messenger observation campaigns for gravitational wave follow-ups.

We describe a practical approach that uses Multi-Order Coverage (MOC) maps [17] to describe regions on the sky that are observable from given locations on the Earth, taking into account specific constraints on the airmass values and the time allocated for the observation. The identification of existing image data is an integral part of this process, which also benefits significantly from the MOC based approach. Operationally, this approach uses Python modules for the creation and manipulation of MOCs (`mocpy`; [18], [19]) and for use of the HEALPix tessellation [20] (`cds-healpix-python`; [21]), combined with the `astroplan` package [22] to select the HEALPix indices at a given order and to set up a new MOC map that represents the visibility with all of these constraints taken into account. Note that the complete code is reported in a public GitHub repository⁴ which indicates all of the Python modules necessary for this analysis. A video demonstration⁵ is also provided focusing on the Aladin functionalities used through the paper.

2. Multi Order Coverage Map (MOC)

The MOC encoding method was originally developed at the Centre de Données astronomiques de Strasbourg (CDS) and has been adopted as a recommendation by the IVOA as the MOC 1.0 standard [23] and updated with the MOC 1.1 standard [17]. Initially designed for manipulating sky coverages from astronomical surveys, MOC is currently being extended to support both temporal and spatial coverage in the MOC 2.0 standard [24] that is currently at the "Proposed Recommendation" status in the IVOA standardisation process. MOC 2.0 considers space MOCs (SMOC), time MOCs (TMOC) and the combined space-Time MOC (STMOC).

The ability to transform any spatial MOC generated from telescope footprints, image surveys, catalogues, gravitational-wave sky localizations, MOC visibility etc. into spatial and temporal MOC (STMOC) [24] could have an impact both in immediate collaboration and sharing between different networks and in archival searches to investigate the current theoretical models (see **Fig. 4** in [24]). This paper concerns mainly space MOCs (which we refer to simply as MOCs) with a small application of the STMOC.

MOCs are a very useful mechanism to improve the efficiency of querying VO services. A number of services support queries based on MOCs in different ways. For example the CDS VizieR service allows catalogues of astronomical sources to be queried by MOC to provide a list of sources within the MOC. Another example is the use of MOCs in the 20 HiPS node sites, where the MOC file (as described in the HiPS standard - [25]) can be used to avoid loading any HiPS

⁴<https://github.com/ggreco77/MOC-to-plan-MMA>

⁵https://virgo.pg.infn.it/sites/virgo.pg.infn.it/files/mm/tuto_A_C_mid.mp4

tiles located outside the coverage of the HiPS data. Furthermore the CDS MOC Server⁶ includes the MOCs of ~ 27000 image and catalogue data sets, which can help by providing a way to limit queries only to data sets that have coverages in the sky region of interest. Such considerations help optimise the response times of data searches which can be critical in planning of observations.

2.1. A brief description of MOC

The MOC data structure is based on the HEALPix (**H**ierarchical **E**qual **A**rea iso**L**atitude **P**ixelization) sky tessellation algorithm [20]. In its base partitioning, a HEALPix sphere is hierarchically tessellated into curvilinear quadrilaterals. The lowest resolution partition consists of twelve base pixels. The resolution of the tessellation, indicated by the parameter n_{side} , increases by division of each pixel into four new ones. The number of pixels composing the sphere at a specific resolution is $12 \times n_{side}^2$.

The fundamental element of a MOC data structure is the HEALPix *cell* which uniquely defines a region on the sky. Each MOC cell is defined by two HEALPix properties: the hierarchy level (HEALPix *order*) and the pixel index (HEALPix *npix*). The finest level of refinement within the MOC hierarchy is determined by the HEALPix order parameter or the equivalent n_{side} ; *order* and n_{side} are related by

$$n_{side} = 2^{order}. \quad (1)$$

For example, $order = 9$ corresponds to $n_{side} = 512$, and a resolution of 6.9' per pixel.

2.2. Serialisations

Two main serialisations of a MOC are supported: JSON and FITS. Serialisations are defined in the MOC standard document [23] (see sections **2.3.2** (FITS) and **3.1.1** (JSON))

A JSON MOC is written following the syntax:

$$\{ "order" : [npix, npix, \dots], "order" : [npix, npix \dots], \dots \}. \quad (2)$$

In the example shown in Figure 1, the JSON MOC shown as the shaded region is defined by 4 cells at $order = 8$:

$$\{ "8" : [228210, 228211, 228216, 228217] \}. \quad (3)$$

To encode a MOC in a FITS file, each cell is converted into a single integer using the standard NUNIQ packing scheme (see [23]):

$$uniq = 4 \times (4^{order}) + npix \quad (4)$$

⁶<https://alaska.unistra.fr/MocServer/query>

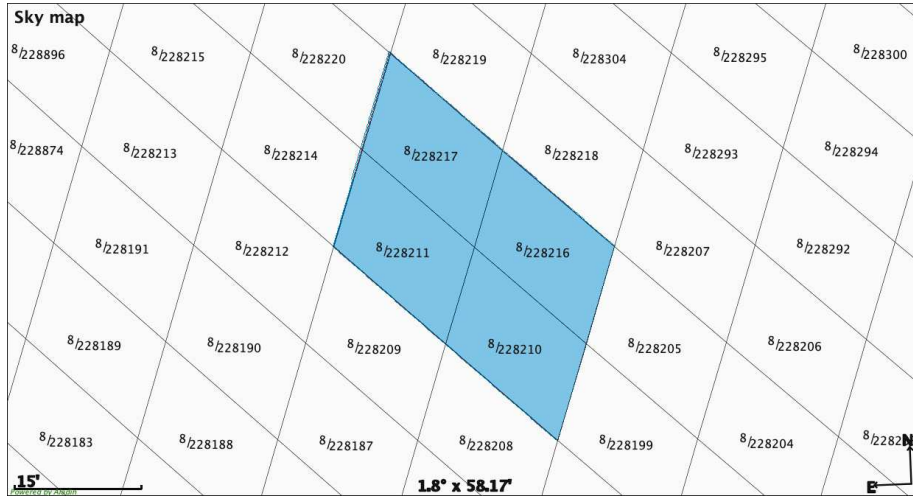


Figure 1: HEALPix grid. The shaded area highlights a MOC map consisting of 4 cells at $order = 8$. Lower-order cells along the edges are not considered here.

In Figure 1, the FITS MOC contains the integers 490354, 490355, 490360, 490361, and the resulting list is stored in a single column binary table extension. The UNIQUE constraint ensures that all values in the column are different. For $order \leq 13$ these UNIQUE values can be stored in a 32-bit signed integer, and for $order \leq 29$ in a 64-bit signed integer.

3. Encoding of 2D credible regions in a MOC map

The 2D credible regions of gravitational-wave sky localizations can be straightforwardly encoded into a MOC data structure [26], [27]. The contours of a gravitational-wave sky localization are constructed following the prescription in [28]: we ranked the pixels from most probable to least, and finally counted how many pixels summed to a given total probability. The algorithm then constructs the MOC coverage extracting the HEALPix pixels inside that contour plot. Every single level of the contained probability can be used as a regular MOC even when the sky localization is irregularly shaped with disjoint regions.

Alternatively, the credible regions can be described by a polygon enclosing a certain percentage of probability. This approach returns an output in which each point is represented by its right ascension and declination and where special terminators are added to delimit disjointed regions if needed. The MOC data structure is more compact, returning a flat list of integers (in a FITS serialisation) and managing the HEALPix resolution (n_{side}) by the MOC order parameter.

Here, the excellent performances of the MOC maps are shown in the context of the multi-messenger science in which data visualisation, data access and data

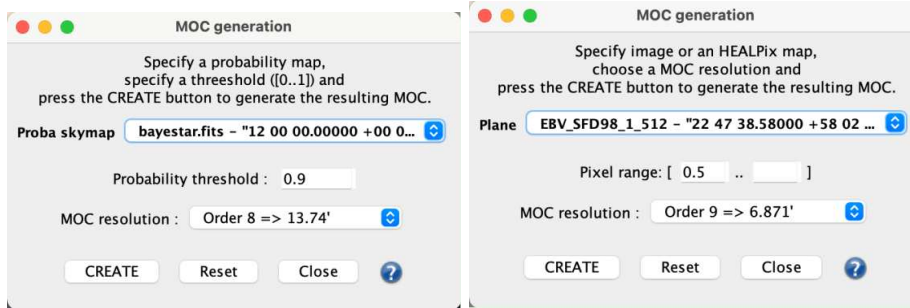


Figure 2: MOC generation windows. The two main Aladin windows which are used to encode a sky region in a MOC data structure. *Left*: from a probability threshold. *Right*: from a collection of pixel values. The sky maps are selected from the dropdown menu **Proba skymap** and **Plane**, respectively. In both windows, the MOC order can be chosen from the dropdown menu **MOC resolution**.

comparison are crucial tasks to search for electromagnetic counterparts from gravitational-wave sources.

In the next section, we demonstrate two tools that can be used to fulfil the task to build MOC data structures from a gravitational-wave sky localization: Aladin Desktop [29] and `ligo.skymap` [30]. These tools support the MOC-encoding process both of the standard HEALPix format (where all the cells are at a single order) and also the multi-resolution HEALPix format [31]⁷ in which different HEALPix orders are included.

3.1. Aladin Desktop

Aladin Desktop is an interactive sky atlas based on Java technology. It was first created in 1999 by the CDS and is regularly updated to be compatible with existing or emerging VO standards. The user-friendly graphical interface is shown in Figure 5. In the left-hand side of the main window is placed the Aladin data collections tree⁸ designed for interactive data access and discovery. The right-hand side is called Aladin stack⁹ and shows all elements that have been loaded during the Aladin Desktop session.

In the Aladin Desktop application a dedicated function is available to generate a credible region at a defined confidence level¹⁰. This is accomplished by selecting the menu bar the item called **Coverage** \Rightarrow **Generate a spatial MOC based on** \Rightarrow **The current probability skymap**.

The MOC generation window, shown in the left panel of Figure 2, offers three options.

⁷https://emfollow.docs.ligo.org/userguide/tutorial/multiorder_skymaps.html

⁸<https://www.youtube.com/watch?v=ggnJ5glhRmA>

⁹https://www.youtube.com/watch?v=-p_nYH42NUo

¹⁰<https://emfollow.docs.ligo.org/userguide/resources/aladin.html>

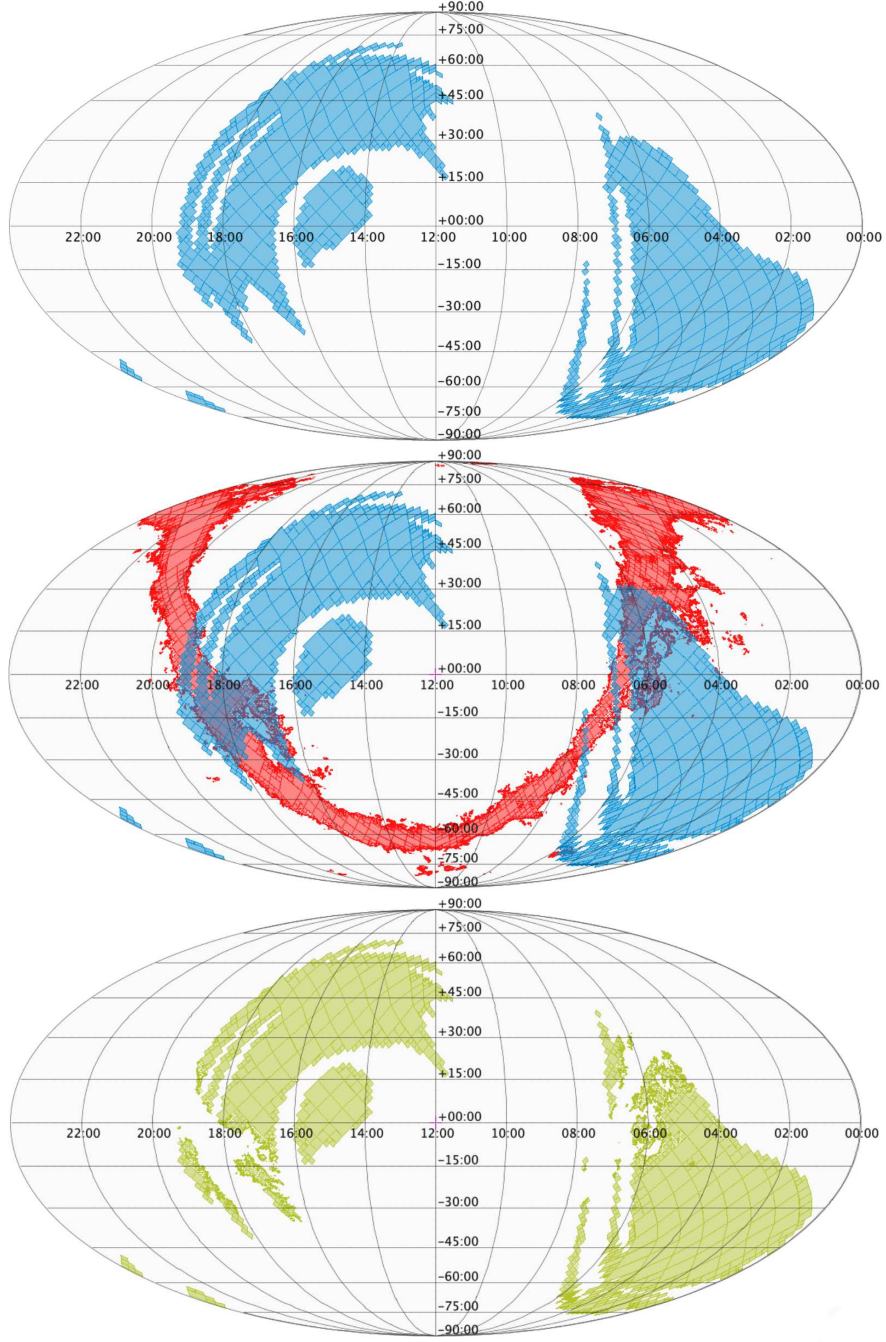


Figure 3: *Top*: Gravitational-wave sky localization of GW190425 - 90% credible region - Mollweide projection. *Middle*: A selected high Galactic dust extinction region is overlaid. The range of pixel values was set from 0.5 up to the highest value. *Bottom*: The resulting sky map defined by the gravitational-wave sky localization with the dust absorption fields subtracted.

- **Proba skymap:** the dropdown menu lists the image files loaded during your Aladin Desktop session. To preselect a gravitational-wave sky localization in the dropdown menu, click on its name in the Aladin Stack.
- **Probability threshold:** a number between 0 and 1 for the credible level you wish to select.
- **MOC resolution:** the dropdown menu lists the MOC-resolution options and the corresponding pixel resolutions. The MOC resolution is related to the *nside* HEALPix parameter following the equation 1.

Pressing the **CREATE** button, the MOC for the credible region is created and loaded in the Aladin Stack. Repetition of this process for different credible levels builds up a set of MOCs that can be selected independently from the Aladin stack.

The main Aladin window shows the credible region over a selected background-image survey for a full interactive visualisation. Among the most important interactive features is the ability to access information on the size of the region. The area in square degrees and the percentage of the sky are shown in the top-right corner of the Aladin stack when you hover the cursor over the MOC name. Alternatively, you can right-click the MOC in the Aladin stack and select **Properties** from the contextual menu.

Finally, the files may be exported via the menu bar item labelled **File** \Rightarrow **Export planes (FITS, VOTable,...)**. The contextual window permits the selection of the relevant planes so that they may be saved in a target directory in various formats (see Subsection 2.2).

3.2. The *ligo.skymap* python package

The *ligo.skymap* package is a set of Python tools for reading, writing, generating, and visualising gravitational-wave probability maps from LIGO and Virgo.

From *ligo.skymap*, it is possible to invoke the command-line `ligo-skymap-contour-moc`¹¹. The method returns a credible level encoded in a MOC data structure of an all-sky probability map in FITS format (see Subsection 2.2).

The method is based on *mocpy*. Recently, the *mocpy* version 0.10.0 builds the credibility regions with an algorithm that has various options, including one which produces the same results as Aladin Desktop, and others that allow for different handling of the region boundaries; see `from_multiordermap_fits_file` method¹².

Mocpy is a Python library allowing easy creation, parsing and manipulation of sky areas encoded in a MOC data structure [32]. Excellent performance in computing time is obtained thanks to the core functions written in Rust

¹¹https://lscsoft.docs.ligo.org/ligo.skymap/tool/ligo_skymap_contour_moc.html

¹²<https://cds-astro.github.io/mocpy/stubs/mocpy.MOC.html>

programming language¹³. The library is part of the affiliated packages of the Astropy project [33], [34].

3.3. MOC data visualisations

MOC maps can be visualised in various environments and libraries. The MOC files can be viewed in the Aladin Desktop or in a dedicated Jupyter Notebook [35] using `ipyaladin`¹⁴. The files may also be viewed in JavaScript applications in which Aladin Lite [36] is embedded. Dedicated tutorials for plotting a general MOC map using the popular Matplotlib library [37] are available in the `mocpy` repository¹⁵.

The property of shading the areas inside the MOC or the property of displaying only the edges are well-suited to display/manage many overlapping planes (see Subsection 5.5).

4. Demonstrations of the utility of MOCs in the preparation of observation campaigns

The scheduling of observational follow-up programs requires many considerations to be taken into account. The primary consideration is the choice of the sky fields which is determined by the credible regions. Here we discuss other constraints that could be taken into account to develop an observing strategy: (i) identifying high Galactic dust extinction areas, and (ii) locating regions in which reference images are already available.

4.1. Application example of GW190425

We apply the method to identify observable sky zones in a MOC map in the context of the low-latency gravitational-wave alert of GW190425 [38]. The event represents the discovery of a second binary neutron star merger after GW170817 [1]. The GW190425 signal has been observed on 2019 April 25, 08:18:05 UTC, during the third observing run (O3) of the LIGO–Virgo network. The network consists of two Advanced LIGO interferometers in Hanford, Washington, USA (LHO) and Livingston, Louisiana, USA (LLO) and the Advanced Virgo interferometer in Cascina, Italy. At the time of GW190425, LHO was temporarily offline with only LLO and Virgo taking data.

The initial sky map, generated by BAYESTAR algorithm [31], has a 90% credible region of 10,183 deg² [39]. It is displayed on the top of Figure 3. Up to the present day, no confirmed electromagnetic or neutrino event has been identified in association with this gravitational-wave event [38].

¹³Release 0.4.1 <https://www.rust-lang.org/>

¹⁴<https://github.com/cds-astro/ipyaladin>

¹⁵<https://github.com/cds-astro/mocpy>

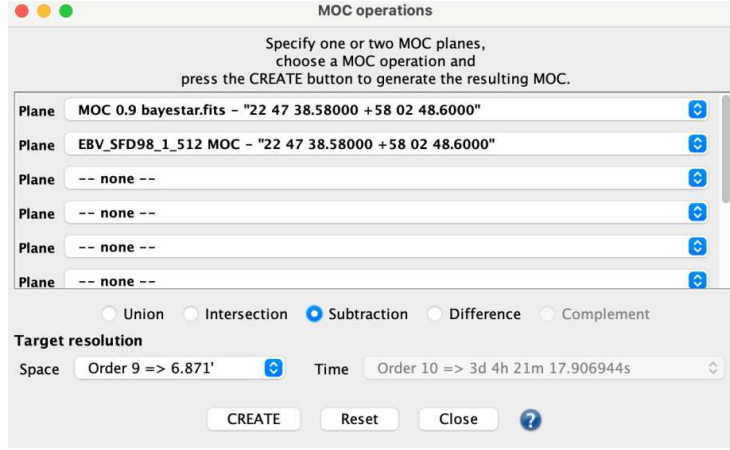


Figure 4: MOC operations. The window provides a set of MOC functions: union, intersection, subtraction and difference for manipulating spatial and/or temporal coverages by selecting the corresponding radio button. The planes are selectable from the dropdown menus. In **Target resolution**, different MOC orders for space and/or time resolutions can be independently chosen.

4.2. Identifying high dust extinction areas

Searches for transient objects generally need to take into account factors that affect the detectability of sources, such as the galactic dust extinction and the stellar density [40], [41]. The algorithm developed by various groups to construct electromagnetic follow-up strategies ([42] [43], [44]) emphasise the impact of dust extinction and stellar density as variables on the detectability of electromagnetic transients associated with gravitational-wave sources. The example described in the present paper is admittedly oversimplified but at the same time provides step-by-step guidelines to customise new results and proper working processes.

For the purpose of the general application, we download the all-sky Galactic reddening map from [45] in HEALPix sky pixelization scheme¹⁶ from the Analysis Center for Extended Data (CADE)¹⁷. The ingestion tool adopted by CADE is based on the drizzling library¹⁸, and applies an algorithm where the surface of pixel intersection is computed as described in [46]. The service delivers VO-compatible data, accessible through the Aladin software.

With the all-sky map of Galactic reddening loaded into Aladin Desktop, the MOC is computed from a pixel range as follows: select **Coverage** \Rightarrow **Generate a spatial MOC based on** \Rightarrow **The current image, HEALPix map or HIPS**. The MOC generation window (shown in the right panel of Figure 2) offers three options.

¹⁶http://cade.irap.omp.eu/dokuwiki/doku.php?id=galactic_reddening

¹⁷<http://cade.irap.omp.eu/dokuwiki/doku.php?id=start>

¹⁸<http://cade.irap.omp.eu/dokuwiki/doku.php?id=software>

- **Plane:** the dropdown menu lists the image files loaded in the Aladin Desktop session. To preselect a plan, click on its name in the Aladin Stack.
- **Pixel range:** a range of pixel values.
- **MOC resolution:** the dropdown menu lists the MOC-resolution options and the corresponding pixel resolutions. The MOC resolution is related to the *nside* HEALPix parameter following the equation 1.

Pressing the **CREATE** button, the resulting MOC is generated and loaded in the Aladin stack.

In this case, we have chosen the range of pixel values from 0.5 up to the highest value, producing an area of 5,472 deg². The resulting MOC from the extinction map, overlapping the original gravitational wave sky localization, is shown in the middle panel of Figure 3.

The operation between the sky areas is performed by selecting **Logical operation** from **Coverage** in the main menu. The window is shown in Figure 4. The **MOC operations** window provides a set of MOC functions: union, intersection, subtraction and difference for manipulating spatial and/or temporal coverages by selecting the corresponding radio button. The planes are selectable from the dropdown menus. In **Target resolution**, you can independently choose different MOC orders for space and/or time resolutions. (For more details in the two-dimensional interleaving approach see Section 3.3 in IVOA Proposed Recommendation [24].)

The resulting coverage map, shown at the bottom panel of Figure 3 depicts the initial sky localization of GW190425 in which certain Galactic reddening values have been subtracted. The operation is computed with a space MOC order = 9. (As no temporal information is stored in those MOCs; the time resolution dropdown menu appears disabled as shown in Figure 4.)

4.3. Searching for reference images

To search for convenient reference images, we explore the public surveys from the Aladin data collections tree¹⁹. When one or more image resources have been chosen, the spatial coverage related to the resource is loaded as a MOC map by checking the box **space cov.** (see Figure 5). This functionality permits further operations to be done with the new MOC map. As a first step, we choose the PanSTARRS DR1²⁰ coverage and then we intersect it with the BAYESTAR gravitational-wave sky localization of GW190425 *pre-processed* as discussed in the previous Section 4.2.

The MOC map of the PanSTARRS DR1 dataset has been generated by CDS as part of the ingestion of the PanSTARRS data into the CDS HiPS node. The MOC was generated using Aladin/HipsGen v10.138.

¹⁹https://www.youtube.com/watch?v=IG_6Eh9EKKk

²⁰<https://panstarrs.stsci.edu/>

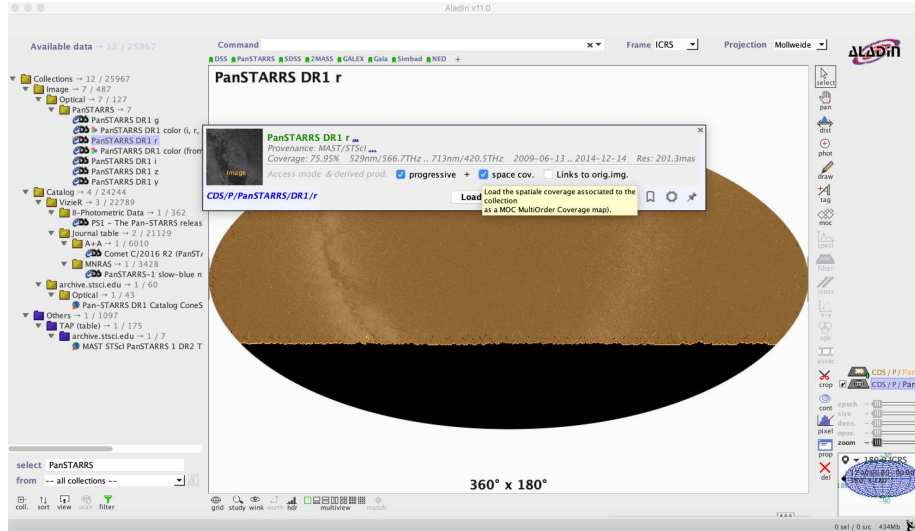


Figure 5: Aladin Graphical User Interface. Left-hand window: exploring the Aladin data collections tree. When a catalogue item has been selected, we can also require to download the spatial coverage associated to the survey as a MOC map checking the box **space cov.**. The data provenance is reported in the same contextual window: **Provenance:** MAST/STScI. By clicking on ..., visualised in the same line, additional information is linked. Left-hand window: Aladin stack. It stacks the loaded planes in an Aladin section.

Figure 6 depicts the MOCs to be used for the operational planning. The top panel shows the PanSTARRS DR1 coverage (in orange) overlapping the initial gravitational-wave sky localization of GW190425 in which dust absorption fields have been removed. The bottom panel displays the intersection area between the two sky coverages. The resulting sky map has been produced by using the **Logical operation** window in Figure 4. The options available in this window are described in Section 4.2. The operation is computed with a space MOC order = 11. No temporal information is stored in that MOCs; the time resolution dropdown menu in Figure 4 will be appear disabled.

This approach provides a very efficient method to identify sky areas in which reference images are available for searching for potential electromagnetic transients associated with a gravitational-wave source. In Section 5.4, we will describe how to gather images when the MOC operations have been concluded according to strategies adopted in an electromagnetic follow-up, and the visibility from an observational site is computed.

5. Determining multi-observability within a MOC coverage

Here we describe the essential steps to delimit portions of a MOC coverage that are observable from a specific astronomical site within a fixed time interval and a defined range of airmass values. For this example, we start with the MOC

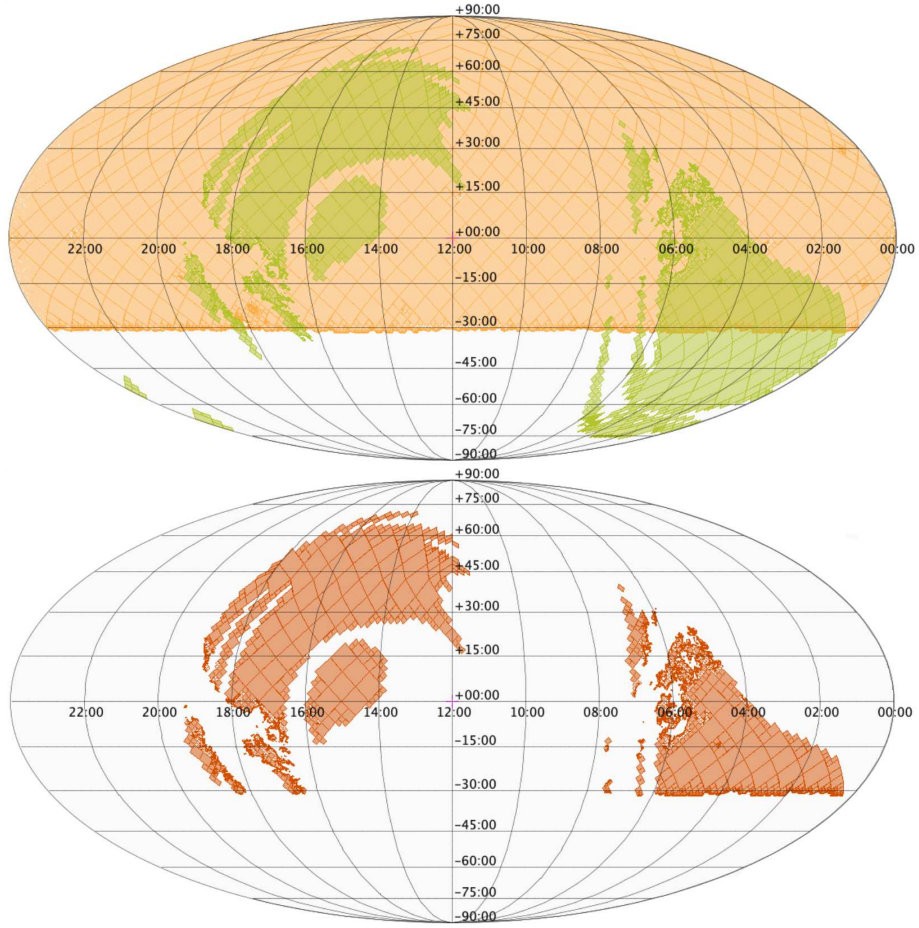


Figure 6: *Top.* In orange the PanSTARRS DR1 coverage of $31,330 \text{ deg}^2$ overlapping the gravitational-wave sky localization of GW190425 in which dust absorption fields have been removed. *Bottom.* The resulting intersection area of $6,777 \text{ deg}^2$ (MOC order = 11).

that was described in the previous section. The complete code is reported in a public GitHub repository in which a jupyter notebook is provided²¹.

5.1. Flattening a MOC map at a fixed order

A MOC object is a collection of cells, originated from the HEALPix tessellation, and stored at different *orders*. In fact, the list of cells is compressed by replacing any four consecutive cells at *order* k by their parent cells from *order* $k - 1$. This operation can be done recursively down to $k = 0$. The deepest level is set by the resolution required for describing the data set [17].

For some purposes, it is more convenient to operate on a "flattened" MOC where all of the cells are at the same order. To calculate the airmass in sky regions with equal areas, we flatten the spatial MOC map to a predefined *order*. MOC uses the NESTED numbering scheme and, thus, each spatial MOC cell can be stored as one single interval ranging from $[npix \times 4^{(max_order - order)}]$ to $[(npix + 1) \times 4^{(max_order - order)} - 1]$. The maximum order of a spatial MOC cell is $max_order = 29$.

In this example, we use the MOC input region serialised in a JSON format. Subsequently, the JSON file is read as an ordinary Python dictionary with the *keys* and *values* representing the *orders* and the *pixel indexes*, respectively.

5.2. From MOC cells to sky coordinates

When the entire collection of cells in a MOC map is flattened to the same order, we invoke from `cds-healpix-python` module the `healpix_to_skycoord` method [47]. This method converts HEALPix indices to celestial coordinates. The input is a 1-D array of HEALPix indices and the resulting celestial coordinates are returned in a **SkyCoord** high-level object as defined in `astropy` [34].

5.3. Computing the visibility of MOC regions from observatory sites

The Python module `astroplan` [22] is used to compute the visibility of a MOC from different observatories by specifying the location and the airmass constraints.

We consider a multi-messenger team composed of three astronomical research observatories: 1) Haleakala Observatories in Hawaii, USA 2) Paranal Observatory in Chile 3) Siding Spring Observatory (SSO) in Australia. With `astroplan` we define three *Observer* classes. *Observer* is an `astroplan` container class for information about an observer's site²².

Using the methods `at_night`, we verify if it is night at the time of the GW190425 at Haleakala Observatories, otherwise, we ask for the nearest twilight astronomical evening with `twilight_evening_astronomical` method.

²¹<https://l.infn.it/tuto-moc-mma>

²²<https://astroplan.readthedocs.io/en/latest/api/astroplan.Observer.html>

Then we calculate the airmass in steps of two hours for each **SkyCoord** as described in **3.1.4** of astroplan documentation²³.

We create a three-column astropy table that merges **SkyCoord** and the related airmass measurements. The resulting table is filtered to specify cases where airmass values are in the range from 1 to 2. Finally, using **from_skycoords** method in **mocpy**, we recreate a new MOC which we refer to as the visibility MOC. We repeat the same steps for Paranal and SSO observatories fixing the same starting time as in the Haleakala site. Figure 7 shows the resulting MOC visibilities from 08:18:05 UTC to 14:18:05 UTC, from top to bottom, in two hour steps for each astronomical observatory.

Table 1 summarises the sky areas of the MOCs and Table 2 lists their overlaps in square degrees. As indicated by the blank values in the second column of Table 2 there are no simultaneous overlaps between all three observatories at any time, but columns 3 and 4 show significant intersections between Haleakala and Paranal, and Haleakala and SSO. The generations of these simple tables allow organising strategies among several observers. Continuing the illustration of this example, to optimise the observations planning in such a case, the intersection areas can be totally subtracted from Haleakala schedule and redistributed between Paranal and SSO observatories. Viceversa, for transient classifications, the same sky regions can be monitored at different wavelengths or instruments ([48], [49]).

5.4. Retrieving the reference images

The images available via the Aladin data collections tree are HiPS (Hierarchical Progressive Survey, [50]) data sets that comply with the IVOA HiPS standard [25]. The HiPS network is made up of 20 nodes hosted at different sites, and a listing of all of the data sets published in the network (more than 900 data sets) is available²⁴. The provenance of each HiPS data set is included in the standardised metadata in the properties file of each data set. Cut-out images, in the FITS (Flexible Image Transport System) format, may be extracted from HiPS data sets using the online hips2fits service [51]²⁵. This provides a very efficient and flexible way to generate cut-outs from many surveys, which can be useful for many purposes albeit with a number of caveats. Note that the extracted FITS files do differ from the original data because they have been converted to HiPS which involves re-sampling onto the HEALPix grid, and then extracted with user-defined sampling into a FITS cut-out by hips2fits. These transformations would need to be taken into consideration when making scientific measurement from these FITS files.

The tiling patterns to split the sky areas proportional to the instrument footprints can also be generated using the Aladin Desktop functionality (from **File** \Rightarrow **Load Instrument FoV** \Rightarrow **Server selector**) or dedicated packages;

²³Release 0.4.1 https://astroplan.readthedocs.io/_/downloads/en/v4.1/pdf/

²⁴<https://aladin.u-strasbg.fr/hips/list>

²⁵<http://alasky.u-strasbg.fr/hips-image-services/hips2fits>

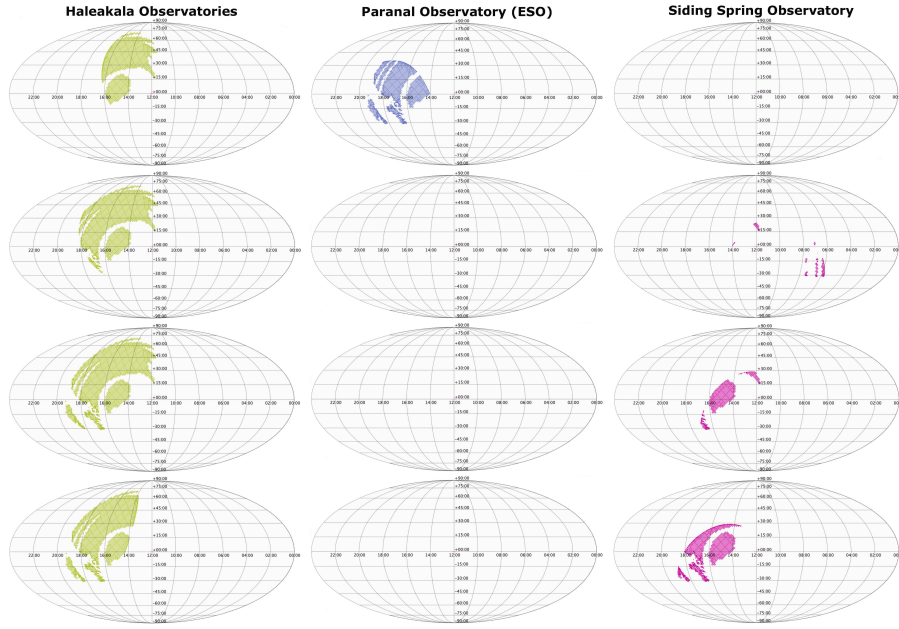


Figure 7: MOC observabilities of the gravitational-wave sky localization of GW190425. The original sky map was previously processed taking into account the all-sky Galactic reddening map from [45] and overlapping the PanSTARRS DR1 survey as reference images. The visibility refers to three astronomical observatories: Haleakala Observatories in Hawaii (USA), Paranal Observatory in Chile and Siding Spring Observatory (SSO) in Australia. The time interval is defined from 08:18:05 UTC to 14:18:05 UTC, from top to bottom, in two hour steps with airmass $1 \leq X \leq 2$.

GWsky²⁶, teglon²⁷, gwemopt²⁸, GW-Localization-Tiling²⁹, sky_tiling³⁰, to mention a few. Three screenshots taken from the video tutorial associated with the present paper compose Figure 5.4. The server selector window, in which the instrument field-of-view can be chosen/added, is shown in the top panel. Two field-of-view footprints are plotted in blue and orange ($1^\circ \times 1^\circ$). The sky position centred at the field-of-view instrument can be taken opening the properties window associated with the current field-of-view instrument loaded in the Aladin stack. That is depicted in the middle panel. Finally the cut-out images can be obtained by filling out the form of the hips2fits web server as shown in the bottom panel.

Note, thumbnails for a list of targets or coordinates are also readily available through the submission of queries from dedicated Python scripts.

5.5. Updating Sky localizations

Gravitational-wave sky localizations are distributed for a single event increasing accuracy and consequently the computational time [52]. The sequence of LIGO/Virgo alerts disseminated through the Gamma-ray Coordinates Network (GCN), during the first Open Public Alert, are described in the LVC User Guide in the Section Alert Timeline³¹.

Figure 9 shows the 90% confidence region from the low-latency sky localization algorithm BAYESTAR in blue, as previously shown in the top panel of Figure 3, overlapping the sky localization published in GWTC-2 (The second Gravitational Wave Transient Catalogue) [53], in magenta. The shaded areas, useful for quick visual comparisons, are obtained using as drawing methods **perimeter** and **fill** in Properties window: right-click the MOCs in the Aladin stack and select **Properties** from the contextual menu.

5.6. Encoding time information in (visibility) MOCs

Operationally, the addition of time information in a spatial MOC can be achieved using the `from_spatial_coverages` method in `mocpy` or managing the **Properties** window in the Aladin Desktop. This is accomplished by selecting the menu bar the item called **Coverage** \Rightarrow **Generate a Space-Time MOC based on** \Rightarrow **The selected Space MOC**.

The resulting new data structure is indicated with STMOC (Space and Time MOC). While a detailed description of STMOC is beyond the scope of this paper, we provide a brief outline based on [24]. The temporal coverage (TMOC) of a data set can be expressed using a discrete time axis where the unit element has a duration of 1 microsecond. Using the same hierarchical approach as the spatial MOCS, the time axis is organised into orders of increasing temporal

²⁶<https://github.com/ggreco77/GWsky>

²⁷<https://github.com/davecoulter/teglon>

²⁸<https://github.com/mcoughlin/gwemopt>

²⁹<https://github.com/kauui8school/GW-Localization-Tiling>

³⁰https://github.com/shaonghosh/sky_tiling

³¹<https://emfollow.docs.ligo.org/userguide/index.html>

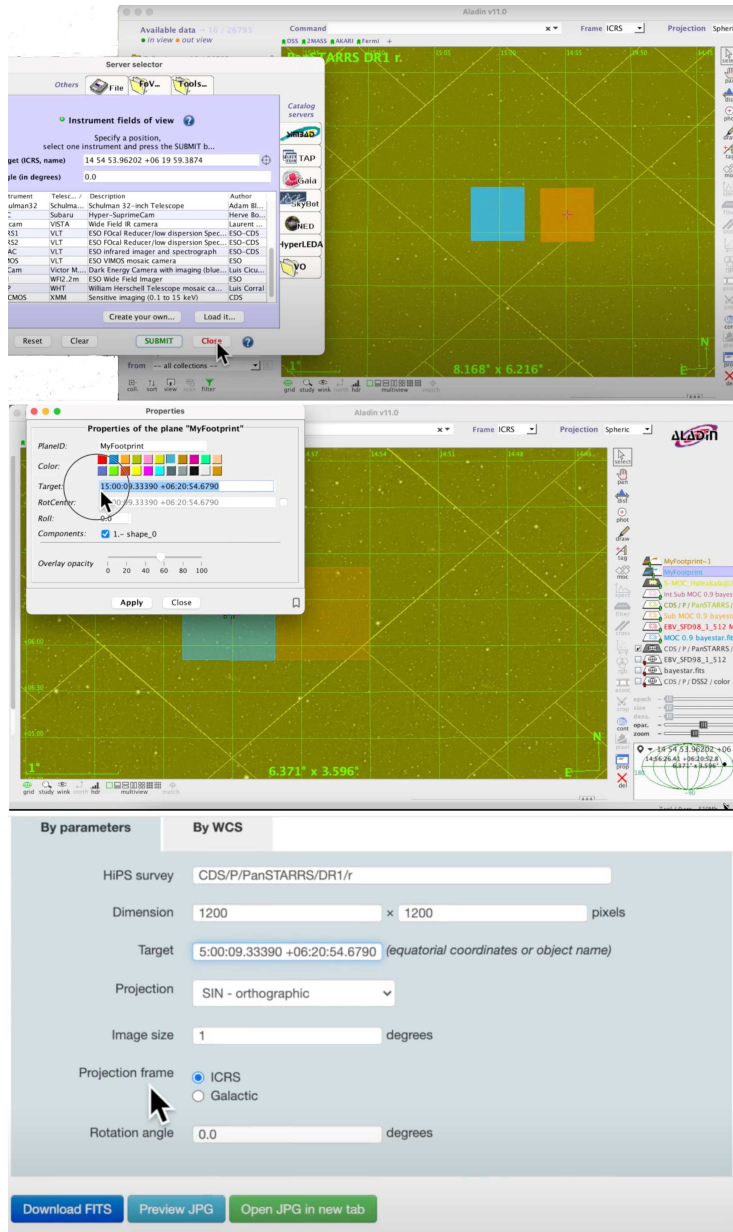


Figure 8: Tiling a sky region and retrieving the images. Two field-of-view footprints ($1^\circ \times 1^\circ$) are plotted in blue and orange. Top: the server selector window in which you can choose/add a field-of-view instrument. Middle: properties window associated with the current field-of-view instrument loaded in the Aladin stack. The box Target shows the sky position centred at the field-of-view instrument. Bottom: web user interface of the hips2fits server. <https://alasky.u-strasbg.fr/hips-image-services/hips2fits>

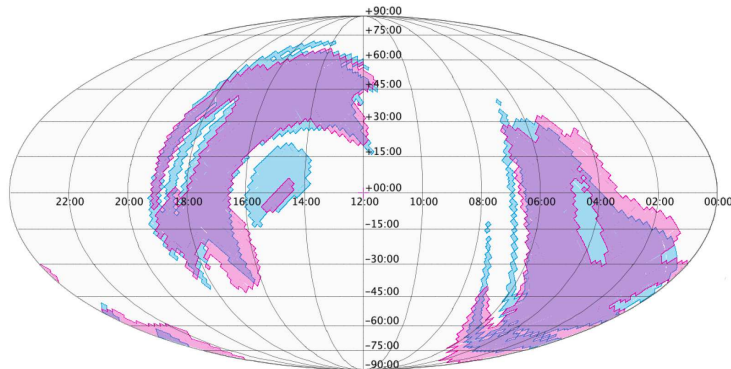


Figure 9: Sky localizations of GW190425. Low-latency sky localization, in light blue, overlapping the sky localization published in GWTC-2, in magenta.

duration, with each order being a factor of two longer than the previous one. Using 62 orders thus enables temporal coverage spanning ~ 73000 years (from $JD=0$) at 1 microsecond resolution. STMOC is the combination of TMOC and the spatial MOC, using a two-dimensional interleaving method for combining the indices and keeping the spatial and temporal coverage resolutions independent.

In the associated tutorial, we make use of the implementation of STMOC in `mocpy` to simultaneously filter a list of transient candidates according to the spatial and temporal information encoded through STMOC.

6. Summary and further developments

Recently, discussions on telescope coordination have been held by the IAU (International Astronomical Union) Executive Committee Working Group on Coordination of Ground and Space Astrophysics organised, with the support of the Kavli Foundation. As a result of a Kavli-IAU Workshop³² a white paper was written summarising the discussions that took place and a set of recommendations and best practises for the community [54]. The development of standards adopted by the community are critical to ensure that heterogeneous transient/multi-messenger systems can communicate efficiently and effectively at a degree of cooperation not currently practised.

The success of recent visualisation packages such as The Gravitational Wave Treasure Map deserves to be mentioned in this framework [55]. It aims to efficiently organise the multi-messenger effort provided by worldwide collaborations (see instruments reporting³³) in order to minimise unnecessary overlap.

In this paper, we have shown various applications for managing the 2D sky maps from source localizations of gravitational-wave transient events when the

³²<https://www.iau.org/news/announcements/detail/ann20027/>

³³<http://treasuremap.space/>

enclosed probability areas are encoded with MOC data structures. We have demonstrated that the MOC data structure to plan multi-messenger observations proves to be a very flexible and interoperable methodology to satisfy many research demands in multi-messenger science (data comparison, data access and data visualisation).

In the Python implementation of MOC, excellent performances are obtained thanks to the core functions written in Rust programming language. Visualisation and operations of MOCs are fully integrated in the VO standard and traditional tools as Aladin Desktop and Aladin Lite. Dedicated software are also developed to share proprietary images or footprints in the HiPS/MOC data structure³⁴ in order to apply the FAIR (Findable, Accessible, Interoperable, Reusable) principles in the context of the IVOA ecosystem.

In more detail, we have investigated an interoperable approach to determine the observability of MOC cells based on the geographic coordinates of ground-based observatories. Before identifying the visibility MOC area, the sky localizations can be processed in order to optimise follow-up strategies to increase the chance to identify the electromagnetic counterpart of a gravitational-wave event. Here we have simulated two basic examples: removing or identifying the highest extinction areas and collecting information querying VO data providers to search for reference image catalogues. In the first operation, we perform a subtraction between the initial gravitational wave sky localization and a dust Galactic map. In the second operation, the subtracted sky map is intersected with the reference image catalogue chosen from the Aladin data trees. The computation speed (generally a few milliseconds, see Section 1.6.4 in [17]) is exceptionally high for the MOC operations. This aspect makes them more efficient than using polygons to confine complex and irregular sky regions.

The visibility of the resulting sky map is quantified from three astronomical sites composing our ideal multi-messenger network.

Finally, we also encoded to the MOC map the temporal information adopting the STMOC data structure. An observation campaign that makes use of visibility (ST)MOCs can easily quantify the observation time between the various observers as soon as an alert has been launched and reshape it in real time meeting the current observational requirement.

The complete code is reported in a jupyter notebook which indicates all of the Python modules necessary for this analysis.

More convenient approaches, especially for instruments with relatively small field of view, can exploit 3D sky maps [56] ranking galaxies inside the 90% of volume with astrophysical prescriptions to trace potential host galaxies for binary mergers that contain a neutron star [57], [58], [59], [60], [61] [62], [63]. These approaches are highly sensitive to the completeness of catalogues [43]. Dedicated interactive web pages have been published to provide access to galaxy lists such as: MANGROVE (Mass Association for GRavitational waves Ob-

³⁴<https://aladin.u-strasbg.fr/hips/HipsIn10Steps.gml>

servations Efficiency)³⁵, NED Gravitational Wave Follow-up (GWF) Service³⁶ and HOGWARTs (Hunt Of Gravitational Wave Areas for Rapid Transients)³⁷.

One of the possible future developments of this work may be to enable the creation of MOC maps based on 3-D gravitational-wave sky localizations. The work presented here has been based on the 2-D probability maps, but this can potentially be extended to 3-D via use of additional information in the LIGO-Virgo-KAGRA sky maps. In future work we will explore the use of additional layers dedicated to measure the conditional distance distribution along a line of sight and extract the galaxies within the 90% credible volume. The idea is to convert the galaxy list "from 3d sky map" in a catalogue HiPS.

Table 1: MOC visibility areas [deg²].

Obs Time (UTC)	Haleakala	Paranal	SSO
2019-04-25 08:18:05.0	2567	2038	–
2019-04-25 10:18:05.0	3989	–	126
2019-04-25 12:18:05.0	4334	–	767
2019-04-25 14:18:05.0	3711	–	1500

Table 2: MOC visibility intersection areas [deg²].

Obs Time (UTC)	Haleakala \cap Paranal \cap SSO	Haleakala \cap Paranal	Haleakala \cap SSO	Paranal \cap SSO
2019-04-25 08:18:05.0	–	657	–	–
2019-04-25 10:18:05.0	–	–	31	–
2019-04-25 12:18:05.0	–	–	761	–
2019-04-25 14:18:05.0	–	–	1450	–

Acknowledgements. The research leading to these results has received funding from the European Union’s Horizon 2020 Programme under the AHEAD2020 project (grant agreement n. 871158). This work has been partly supported by the ESCAPE project (the European Science Cluster of Astronomy & Particle Physics ESFRI Research Infrastructures) that has received funding from the European Union’s Horizon 2020 research and innovation programme under the Grant Agreement n. 824064.

References

- [1] B. P. Abbott, R. Abbott, T. D. Abbott, et al., GW170817: Observation of Gravitational Waves from a Binary Neutron Star Inspiral, Phys. Rev. Lett. 119 (2017) 161101. doi:10.1103/PhysRevLett.119.161101.

³⁵<https://mangrove.lal.in2p3.fr/index.php>

³⁶<https://ned.ipac.caltech.edu/uri/NED::GWFOverview/>

³⁷<https://github.com/Lanasalmon/HOGWARTs>

- [2] B. P. Abbott, R. Abbott, T. D. Abbott, et al., Low-latency Gravitational-wave Alerts for Multimessenger Astronomy during the Second Advanced LIGO and Virgo Observing Run, *The Astrophysical Journal* 875 (2) (2019) 161. [arXiv:1901.03310](#), [doi:10.3847/1538-4357/ab0e8f](#).
- [3] B. P. Abbott, R. Abbott, T. D. Abbott, et al., Multi-messenger Observations of a Binary Neutron Star Merger, *The Astrophysical Journal Letters* 848 (2) (2017) L12. [arXiv:1710.05833](#), [doi:10.3847/2041-8213/aa91c9](#).
- [4] M. W. Coughlin, Lessons from counterpart searches in LIGO and Virgo's third observing campaign, *Nature Astronomy* 4 (2020) 550–552. [doi:10.1038/s41550-020-1130-3](#).
- [5] B. P. Abbott, R. Abbott, T. D. Abbott, et al., Prospects for observing and localizing gravitational-wave transients with Advanced LIGO, Advanced Virgo and KAGRA, *Living Reviews in Relativity* 23 (1) (2020) 3. [doi:10.1007/s41114-020-00026-9](#).
- [6] M. Maggiore, C. V. D. Broeck, N. Bartolo, E. Belgacem, D. Bertacca, M. A. Bizouard, M. Branchesi, S. Clesse, S. Foffa, J. García-Bellido, S. Grimm, J. Harms, T. Hinderer, S. Matarrese, C. Palomba, M. Peloso, A. Ricciardone, M. Sakellariadou, Science case for the einstein telescope, *Journal of Cosmology and Astroparticle Physics* 2020 (03) (2020) 050–050. [doi:10.1088/1475-7516/2020/03/050](#).
- [7] F. Acernese, M. Agathos, K. Agatsuma, et al., Advanced Virgo: a second-generation interferometric gravitational wave detector, *Classical and Quantum Gravity* 32 (2) (2015) 024001. [arXiv:1408.3978](#), [doi:10.1088/0264-9381/32/2/024001](#).
- [8] LIGO Scientific Collaboration, et al., Advanced LIGO, *Classical and Quantum Gravity* 32 (7) (2015) 074001. [arXiv:1411.4547](#), [doi:10.1088/0264-9381/32/7/074001](#).
- [9] Y. Aso, Y. Michimura, K. Somiya, M. Ando, O. Miyakawa, T. Sekiguchi, D. Tatsumi, H. Yamamoto, Interferometer design of the KAGRA gravitational wave detector, *Physical Review D* 88 (4) (2013) 043007. [arXiv:1306.6747](#), [doi:10.1103/PhysRevD.88.043007](#).
- [10] D. Reitze, R. X. Adhikari, S. Ballmer, B. Barish, L. Barsotti, G. Billingsley, D. A. Brown, Y. Chen, D. Coyne, R. Eisenstein, M. Evans, P. Fritschel, E. D. Hall, A. Lazzarini, G. Lovelace, J. Read, B. S. Sathyaprakash, D. Shoemaker, J. Smith, C. Torrie, S. Vitale, R. Weiss, C. Wipf, M. Zucker, Cosmic Explorer: The U.S. Contribution to Gravitational-Wave Astronomy beyond LIGO, in: *Bulletin of the American Astronomical Society*, Vol. 51, 2019, p. 35. [arXiv:1907.04833](#).
- [11] M. Punturo, M. Abernathy, F. Acernese, et al., The Einstein Telescope: a third-generation gravitational wave observatory, *Classical and Quantum Gravity* 27 (19) (2010) 194002. [doi:10.1088/0264-9381/27/19/194002](#).

- [12] G. B. Berriman, the IVOA Executive Committee, the IVOA Technical Coordination Group, the IVOA Community, The International Virtual Observatory Alliance (IVOA) in 2020, in: J.-E. Ruiz, P. Federici (Eds.), ADASS XXX, Vol. 525 of ASP Conf. Ser., ASP, San Francisco, 2021.
- [13] M. G. Allen, S. Derriere, F. Bonnarel, T. Boch, P. Fernique, M. Dolensky, M. Louys, A. M. Richards, Virtual observatory standards in action, in: P. J. Quinn, A. Bridger (Eds.), Optimizing Scientific Return for Astronomy through Information Technologies, Vol. 5493, International Society for Optics and Photonics, SPIE, 2004, pp. 153 – 162. doi:10.1117/12.551513.
- [14] A. Schaaff, Data in astronomy: From the pipeline to the virtual observatory, in: M. Weske, M.-S. Hacid, C. Godart (Eds.), Web Information Systems Engineering – WISE 2007 Workshops, Springer Berlin Heidelberg, Berlin, Heidelberg, 2007, pp. 52–62.
- [15] F. Genova, M. G. Allen, C. Arviset, A. Lawrence, F. Pasian, E. Solano, J. Wambsganss, Euro-vo—coordination of virtual observatory activities in europe, Astronomy and Computing 11 (2015) 181–189, the Virtual Observatory: II. doi:<https://doi.org/10.1016/j.ascom.2015.03.001>.
- [16] J. U. Ness, C. Sánchez Fernández, A. Ibarra, R. Saxton, J. Salgado, E. Kuulkers, P. Kretschmar, M. Ehle, E. Salazar, C. Gabriel, M. Perdikias, Towards a better coordination of multimessenger observations., Memorie della Societa Astronomica Italiana 90 (2019) 110.
- [17] P. Fernique, T. Boch, T. Donaldson, D. Durand, W. O’Mullane, M. Reinecke, M. Taylor, MOC - HEALPix Multi-Order Coverage map Version 1.1, IVOA Recommendation 07 October 2019 (Oct. 2019).
- [18] T. Boch, MOCPy, a Python Library to Manipulate Spatial Coverage Maps, in: M. Molinaro, K. Shortridge, F. Pasian (Eds.), Astronomical Data Analysis Software and Systems XXVI, Vol. 521 of Astronomical Society of the Pacific Conference Series, 2019, p. 487.
- [19] M. Baumann, T. Boch, P. Fernique, A. Nebot, F. X. Pineau, Space and Time Coverage Maps in MOCPy, in: R. Pizzo, E. R. Deul, J. D. Mol, J. de Plaa, H. Verkouter (Eds.), Astronomical Society of the Pacific Conference Series, Vol. 527 of Astronomical Society of the Pacific Conference Series, 2020, p. 693.
- [20] K. M. Górski, E. Hivon, A. J. Banday, B. D. Wandelt, F. K. Hansen, M. Reinecke, M. Bartelmann, HEALPix: A Framework for High-Resolution Discretization and Fast Analysis of Data Distributed on the Sphere, The Astrophysical Journal 622 (2) (2005) 759–771. arXiv:[astro-ph/0409513](https://arxiv.org/abs/astro-ph/0409513), doi:10.1086/427976.
- [21] F.-X. Pineau, P. Fernique, The CDS HEALPix Library, in: P. J. Teuben, M. W. Pound, B. A. Thomas, E. M. Warner (Eds.), Astronomical Data

Analysis Software and Systems XXVII, Vol. 523 of Astronomical Society of the Pacific Conference Series, 2019, p. 609.

- [22] B. M. Morris, E. Tollerud, B. Sipőcz, C. Deil, S. T. Douglas, J. Berlanga Medina, K. Vyhmeister, T. R. Smith, S. Littlefair, A. M. Price-Whelan, W. T. Gee, E. Jeschke, *astroplan*: An Open Source Observation Planning Package in Python, *The Astronomical Journal* 155 (3) (2018) 128. [arXiv:1712.09631](#), [doi:10.3847/1538-3881/aaa47e](#).
- [23] P. Fernique, T. Boch, T. Donaldson, D. Durand, W. O’Mullane, M. Reinecke, M. Taylor, MOC - HEALPix Multi-Order Coverage map Version 1.0, IVOA Recommendation 02 June 2014 (Jun. 2014). [arXiv:1505.02937](#), [doi:10.5479/ADS/bib/2014ivoa.spec.0602F](#).
- [24] P. Fernique, A. Nebot, D. Durand, M. Baumann, T. Boch, G. Greco, T. Donaldson, F.-X. Pineau, M. Taylor, W. O’Mullane, M. Reinecke, S. Derrière, MOC: Multi-Order Coverage map Version 2.0. IVOA IVOA Proposed Recommendation 01 November 2021, <https://ivoa.net/documents/MOC/20211101/index.html> (2021).
- [25] P. Fernique, M. Allen, T. Boch, T. Donaldson, D. Durand, K. Ebisawa, L. Michel, J. Salgado, F. Stoehr, Hips - hierarchical progressive survey version 1.0 [doi:10.5479/ads/bib/2017ivoa.spec.0519f](#).
- [26] G. Greco, M. Branchesi, E. Chassande-Mottin, M. W. Coughlin, G. Stratta, G. Dálya, G. Hemming, L. Rei, E. Brocato, P. Fernique, T. Boch, S. Derrière, M. Baumann, F. Genova, M. Allen, Working with Gravitational-Wave sky localizations: new methods and implementations, *PoS Asterics2019* (2019) 031. [doi:10.22323/1.357.0031](#).
- [27] G. Greco, et al., Capability for encoding gravitational-wave sky localizations with the Multi Order Coverage data structure: present and future developments, in: J.-E. Ruiz, P. Federici (Eds.), *ADASS XXX*, Vol. 525 of ASP Conf. Ser., ASP, San Francisco, 2021.
- [28] L. P. Singer, L. R. Price, B. Farr, A. L. Urban, C. Pankow, S. Vitale, J. Veitch, W. M. Farr, C. Hanna, K. Cannon, T. Downes, P. Graff, C.-J. Haster, I. Mandel, T. Sidery, A. Vecchio, The First Two Years of Electromagnetic Follow-up with Advanced LIGO and Virgo, *The Astrophysical Journal* 795 (2) (2014) 105. [arXiv:1404.5623](#), [doi:10.1088/0004-637X/795/2/105](#).
- [29] F. Bonnarel, P. Fernique, O. Bienaymé, D. Egret, F. Genova, M. Louys, F. Ochsenbein, M. Wenger, J. G. Bartlett, The ALADIN interactive sky atlas. A reference tool for identification of astronomical sources, *Astronomy & Astrophysics Supplement* 143 (2000) 33–40. [doi:10.1051/aas:2000331](#).
- [30] L. P. Singer, et al., *ligo.skymap* 0.5.0 documentation, <https://lscsoft.docs.ligo.org/ligo.skymap/> (2020).

- [31] L. P. Singer, L. R. Price, Rapid Bayesian position reconstruction for gravitational-wave transients, *Physical Review D* 93 (2) (2016) 024013. [arXiv:1508.03634](#), [doi:10.1103/PhysRevD.93.024013](#).
- [32] T. Boch, M. Baumann, et al., MOCpy 0.10.0 documentation, <https://cds-astro.github.io/mocpy/> (2021).
- [33] Astropy Collaboration, T. P. Robitaille, E. J. Tollerud, Greenfield, et al., Astropy: A community Python package for astronomy, *Astronomy & Astrophysics* 558 (2013) A33. [arXiv:1307.6212](#), [doi:10.1051/0004-6361/201322068](#).
- [34] Astropy Collaboration, A. M. Price-Whelan, B. M. Sipőcz, Günther, et al., The Astropy Project: Building an Open-science Project and Status of the v2.0 Core Package, *The Astronomical Journal* 156 (3) (2018) 123. [arXiv:1801.02634](#), [doi:10.3847/1538-3881/aabc4f](#).
- [35] T. Kluyver, B. Ragan-Kelley, F. Pérez, B. Granger, M. Bussonnier, J. Frederic, K. Kelley, J. Hamrick, J. Grout, S. Corlay, P. Ivanov, D. Avila, S. Abdalla, C. Willing, Jupyter notebooks – a publishing format for reproducible computational workflows, in: F. Loizides, B. Schmidt (Eds.), *Positioning and Power in Academic Publishing: Players, Agents and Agendas*, IOS Press, 2016, pp. 87 – 90.
- [36] T. Boch, P. Fernique, Aladin Lite: Embed your Sky in the Browser, in: N. Manset, P. Forshay (Eds.), *Astronomical Data Analysis Software and Systems XXIII*, Vol. 485 of *Astronomical Society of the Pacific Conference Series*, 2014, p. 277.
- [37] J. D. Hunter, Matplotlib: A 2D graphics environment, *Computing in Science & Engineering* 9 (3) (2007) 90–95. [doi:10.1109/MCSE.2007.55](#).
- [38] B. P. Abbott, R. Abbott, T. D. Abbott, et al., GW190425: Observation of a Compact Binary Coalescence with Total Mass $\sim 3.4\,m_{\odot}$, *The Astrophysical Journal* 892 (1) (2020) L3. [doi:10.3847/2041-8213/ab75f5](#).
- [39] The LIGO Scientific Collaboration and the Virgo Collaboration, GCN CIRCULAR 24168: LIGO/Virgo S190425z: Identification of a GW compact binary merger candidate, <https://gcn.gsfc.nasa.gov/gcn3/24168.gcn3> (2019).
- [40] E. Brocato, M. Branchesi, E. Cappellaro, A. Grado, G. Greco, L. Limatola, G. Stratta, S. Yang, S. Campana, P. D’Avanzo, F. Getman, A. Melandri, L. Nicastro, E. Palazzi, E. Pian, S. Piranomonte, L. Pulone, A. Rossi, V. Testa, Grawita: VLT survey telescope observations of the gravitational wave sources GW150914 and GW151226, *Monthly Notices of the Royal Astronomical Society* 474 (10 2017). [doi:10.1093/mnras/stx2730](#).

- [41] I. Andreoni, E. C. Kool, A. S. Carracedo, M. M. Kasliwal, M. Bulla, T. Ahumada, M. W. Coughlin, S. Anand, J. Sollerman, A. Goobar, D. L. Kaplan, T. T. Loveridge, V. Karambelkar, J. Cooke, A. Bagdasaryan, E. C. Bellm, S. B. Cenko, et al., Constraining the kilonova rate with zwicky transient facility searches independent of gravitational wave and short gamma-ray burst triggers, *The Astrophysical Journal* 904 (2) (2020) 155. doi:10.3847/1538-4357/abbf4c.
- [42] O. S. Salafia, M. Colpi, M. Branchesi, E. Chassande-Mottin, G. Ghirlanda, G. Ghisellini, S. D. Vergani, Where and When: Optimal Scheduling of the Electromagnetic Follow-up of Gravitational-wave Events Based on Counterpart Light-curve Models, *The Astrophysical Journal* 846 (1) (2017) 62. arXiv:1704.05851, doi:10.3847/1538-4357/aa850e.
- [43] M. W. Coughlin, D. Tao, M. L. Chan, D. Chatterjee, N. Christensen, S. Ghosh, G. Greco, Y. Hu, S. Kapadia, J. Rana, O. S. Salafia, C. W. Stubbs, Optimizing searches for electromagnetic counterparts of gravitational wave triggers, *Monthly Notices of the Royal Astronomical Society* 478 (1) (2018) 692–702. doi:10.1093/mnras/sty1066.
- [44] K. Herner, J. Annis, D. Brout, M. Soares-Santos, R. Kessler, M. Sako, R. Butler, Z. Doctor, A. Palmese, S. Allam, D. Tucker, F. Sobreira, B. Yanny, H. Diehl, J. Frieman, N. Glaeser, A. Garcia, N. Sherman, et al., Optical follow-up of gravitational wave triggers with decam during the first two ligo/virgo observing runs, *Astronomy and Computing* 33 (2020) 100425. doi:https://doi.org/10.1016/j.ascom.2020.100425.
- [45] D. J. Schlegel, D. P. Finkbeiner, M. Davis, Maps of dust IR emission for use in estimation of reddening and CMBR foregrounds, *Astrophys. J.* 500 (1998) 525. arXiv:astro-ph/9710327, doi:10.1086/305772.
- [46] D. Paradis, K. Dobashi, T. Shimoikura, A. Kawamura, T. Onishi, Y. Fukui, J. P. Bernard, Dark gas in the solar neighborhood from extinction data, *Astronomy & Astrophysics* 543 (2012) A103. arXiv:1205.3384, doi:10.1051/0004-6361/201118740.
- [47] F.-X. Pineau, M. Baumann, et al., cdshealpix 0.5.3 documentation, <https://cds-astro.github.io/cds-healpix-python/> (2020).
- [48] A. Antonelli, A. Carosi, B. de Lotto, R. Mirzoyan, A. Stamerra, LIGO/Virgo G211117: MAGIC very-high energy gamma-ray observations., *GRB Coordinates Network* 18776 (2015) 1.
- [49] N. R. Tanvir, K. Wiersema, P. T. O’Brien, J. Osborne, et al., LIGO/Virgo G211117: VISTA imaging, *GRB Coordinates Network* 18842 (2016) 1.
- [50] P. Fernique, M. G. Allen, T. Boch, A. Oberto, F. X. Pineau, D. Durand, C. Bot, L. Cambr sy, S. Derriere, F. Genova, F. Bonnarel, Hierarchical progressive surveys. Multi-resolution HEALPix data structures for astronomical images, catalogues, and 3-dimensional data cubes,

- Astronomy & Astrophysics 578 (2015) A114. [arXiv:1505.02291](#), [doi:10.1051/0004-6361/201526075](#).
- [51] T. Boch, P. Fernique, F. Bonnarel, C. Chaitra, C. Bot, F. X. Pineau, M. Baumann, L. Michel, HiPS2FITS: Fast Generation of FITS Cutouts From HiPS Image Datasets, in: R. Pizzo, E. R. Deul, J. D. Mol, J. de Plaa, H. Verkouter (Eds.), Astronomical Society of the Pacific Conference Series, Vol. 527 of Astronomical Society of the Pacific Conference Series, 2020, p. 121.
 - [52] B. P. Abbott, R. Abbott, T. D. Abbott, et al., Localization and Broad-band Follow-up of the Gravitational-wave Transient GW150914, *The Astrophysical Journal Letters* 826 (1) (2016) L13. [arXiv:1602.08492](#), [doi:10.3847/2041-8205/826/1/L13](#).
 - [53] R. Abbott, T. D. Abbott, S. Abraham, et al., GWTC-2: Compact Binary Coalescences Observed by LIGO and Virgo during the First Half of the Third Observing Run, *Physical Review X* 11 (2) (2021) 021053. [arXiv:2010.14527](#), [doi:10.1103/PhysRevX.11.021053](#).
 - [54] S. B. Cenko, P. A. Whitelock, L. Cadonati, V. Connaughton, R. Davies, R. Fender, P. J. Groot, M. M. Kasliwal, T. Murphy, S. Nissanke, A. Sesana, S. Yoshida, B. Zhang, International Coordination of Multi-Messenger Transient Observations in the 2020s and Beyond: Kavli-IAU White Paper, *arXiv e-prints* (Jul. 2020). [arXiv:2007.05546](#).
 - [55] S. D. Wyatt, A. Tohuvavohu, I. Arcavi, M. J. Lundquist, D. A. Howell, D. J. Sand, The Gravitational Wave Treasure Map: A Tool to Coordinate, Visualize, and Assess the Electromagnetic Follow-up of Gravitational-wave Events, *The Astrophysical Journal* 894 (2) (2020) 127. [arXiv:2001.00588](#), [doi:10.3847/1538-4357/ab855e](#).
 - [56] L. P. Singer, H.-Y. Chen, D. E. Holz, W. M. Farr, L. R. Price, V. Raymond, S. B. Cenko, N. Gehrels, J. Cannizzo, M. M. Kasliwal, S. Nissanke, M. Coughlin, B. Farr, A. L. Urban, S. Vitale, J. Veitch, P. Graff, C. P. L. Berry, S. Mohapatra, I. Mandel, GOING THE DISTANCE: MAPPING HOST GALAXIES OF LIGO AND VIRGO SOURCES IN THREE DIMENSIONS USING LOCAL COSMOGRAPHY AND TARGETED FOLLOW-UP, *The Astrophysical Journal* 829 (1) (2016) L15. [doi:10.3847/2041-8205/829/1/L15](#).
 - [57] L. P. Singer, H.-Y. Chen, D. E. Holz, W. M. Farr, L. R. Price, V. Raymond, S. B. Cenko, N. Gehrels, J. Cannizzo, M. M. Kasliwal, S. Nissanke, M. Coughlin, B. Farr, A. L. Urban, S. Vitale, J. Veitch, P. Graff, C. P. L. Berry, S. Mohapatra, I. Mandel, SUPPLEMENT: “GOING THE DISTANCE: MAPPING HOST GALAXIES OF LIGO AND VIRGO SOURCES IN THREE DIMENSIONS USING LOCAL COSMOGRAPHY AND TARGETED FOLLOW-UP” (2016, *ApJL*, 829,

- 115), *The Astrophysical Journal Supplement Series* 226 (1) (2016) 10. doi:10.3847/0067-0049/226/1/10.
- [58] N. Gehrels, J. K. Cannizzo, J. Kanner, M. M. Kasliwal, S. Nissanke, L. P. Singer, Galaxy Strategy for LIGO-Virgo Gravitational Wave Counterpart Searches, *The Astrophysical Journal* 820 (2) (2016) 136. arXiv:1508.03608, doi:10.3847/0004-637X/820/2/136.
- [59] E. Antolini, I. Caiazzo, R. Davé, J. S. Heyl, Using galaxy formation simulations to optimize LIGO follow-up observations, *Monthly Notices of the Royal Astronomical Society* 466 (2) (2017) 2212–2216. arXiv:1612.04412, doi:10.1093/mnras/stw3292.
- [60] I. Arcavi, C. McCully, G. Hosseinzadeh, D. A. Howell, S. Vasylyev, D. Poznanski, M. Zaltzman, D. Maoz, L. Singer, S. Valenti, D. Kasen, J. Barnes, T. Piran, W. fai Fong, Optical follow-up of gravitational-wave events with las cumbres observatory, *The Astrophysical Journal* 848 (2) (2017) L33. doi:10.3847/2041-8213/aa910f.
- [61] J. Rana, K. P. Mooley, Galaxy-Targeting Approach Optimized for Finding the Radio Afterglows of Gravitational Wave Sources, arXiv e-prints (Apr. 2019). arXiv:1904.07335.
- [62] J.-G. Ducoin, D. Corre, N. Leroy, E. Le Floch, Optimizing gravitational waves follow-up using galaxies stellar mass, *Monthly Notices of the Royal Astronomical Society* 492 (4) (2020) 4768–4779. doi:10.1093/mnras/staa114.
- [63] M. C. Artale, Y. Bouffanais, M. Mapelli, N. Giacobbo, N. B. Sabha, F. Santoliquido, M. Pasquato, M. Spera, An astrophysically motivated ranking criterion for low-latency electromagnetic follow-up of gravitational wave events, *Monthly Notices of the Royal Astronomical Society* 495 (2) (2020) 1841–1852. doi:10.1093/mnras/staa1252.